Light Directs Monomer Coordination in Catalyst-Free Grignard Photopolymerization

Eliot F. Woods,[1] Alexandra J. Berl,[1] Leanna P. Kantt,[1] Christopher T. Eckdahl,[1] Michael R. Wasielewski,[1] Brandon E. Haines,[2]* and Julia A. Kalow[1]*

[1]Department of Chemistry, Northwestern University, 2145 Sheridan Rd, Evanston, IL 60208

[2]Department of Chemistry, Westmont College, 955 La Paz Rd, Santa Barbara, CA 93108.

ABSTRACT: π-Conjugated polymers can serve as active layers in flexible and lightweight electronics, and are conventionally synthesized by transition-metal-mediated polycondensation at elevated temperatures. We recently reported a photopolymerization of electron-deficient heteroaryl Grignard monomers that enables the catalyst-free synthesis of n-type π-conjugated polymers. Herein we describe an experimental and computational investigation into the mechanism of this photopolymerization. Spectroscopic studies performed in situ and after quenching reveal that the propagating chain is a radical anion with halide end groups. DFT calculations for model oligomers suggest a Mg-templated $S_{RN}1$-type coupling, in which Grignard monomer coordination to the radical anion chain avoids the formation of free sp^2 radicals and enables C–C bond formation with very low barriers. We find that light plays an unusual role in the reaction, photoexciting the radical anion chain to shift electron density to the termini and thus favor productive monomer binding.

Introduction

π-Conjugated polymers (CPs) are primarily synthesized using thermal transition-metal-mediated cross-coupling reactions.[1] Despite the efficiency of these polycondensations, the transition-metal catalysts are challenging to remove and negatively impact device performance.[2–5] New methods have been developed to overcome the limitations of conventional polycondensations through distinct mechanisms. Recently, there have been several reports detailing photochemical routes to CPs, including protocols that eliminate transition metals.[6–9] Photochemical methods have largely been applied to electron-rich (p-type) CPs, while reactions that provide electron-poor (n-type) CPs have lagged.[10,11] For devices that use CPs, such as flexible electronics and lightweight solar cells, both high performance p-type and n-type materials are required.[12] New reactions and a deeper understanding of their mechanisms will improve the utility of CPs. To expand synthetic access to n-type conjugated polymers, we developed the photopolymerization of electron-poor aryl Grignard monomers using visible light (Figure 1a).[13] This polymerization has characteristics consistent with an uncontrolled chain-growth mechanism, allowing us to synthesize a fully conjugated n-type block copolymer.

Several aspects of this light-mediated polymerization merited further study. In contrast to other Kumada polycondensations, this reaction proceeds without a transition-metal catalyst, requiring only lithium chloride (LiCl)-saturated THF and light. Dark control reactions yielded oligomers (degree of polymerization, DP < 5), and higher-molecular-weight polymers were only produced with visible light irradiation (Figure 1b). LiCl was also found to be essential to achieve higher molecular weights and yields. While Grignard reagents and LiCl are known to form reactive "turbo Grignards" in solution,[14,15] the improvements in reaction performance required well beyond the stoichiometric quantities of LiCl needed to form such complexes, suggesting a more nuanced role in the reaction (Figure 1c). Finally, the photopolymerization proved compatible with several n-type homopolymers and donor-acceptor polymers, but when applied to common electron-rich monomers, such as 3-hexylthiophene, produced only trace oligomer (Figure 1d).

Previous work has described the catalyst-free cross-coupling reaction between aryl Grignards and aryl halides as a radical-nucleophilic aromatic substitution process ($S_{RN}1$ reaction).[16,17] Unlike our polymerization, reactions that access small-molecule biaryls and meta-linked poly(arylenes) rely on high temperatures instead of light. Hayashi used radical clock experiments to rule out free aryl radical intermediates in the small-molecule coupling reaction; furthermore, authentic aryl radicals generated from diazonium salts overwhelmingly underwent hydrogen atom transfer rather than C–C bond formation.[16] A computational investigation by Haines and Wiest[18] provided an explanation for the absence of detectable free aryl radical intermediates. In their proposed mechanism (Scheme 1), coordination of the aryl Grignard to the aryl halide radical anion allows the resulting aryl radical intermediate to be captured by Mg^{2+} in an ion-radical cage. Collapse into a new Csp^2–Csp^2 bond occurs rapidly. All the proposed steps after rate-determining SET were found to have very low barriers (< 3 kcal/mol).

Herein we report an experimental and computational mechanistic study of the photocontrolled synthesis of n-type conjugated polymers, revisiting the Grignard-directed $S_{RN}1$ mechanism in the context of our polymerization. Differences between the small-molecule system and the polymer system explain key experimental observations such as the need for photoexcitation, LiCl, and the preference for electron-poor polymers. We uncover an unusual example of a photocontrolled reaction in which light redistributes electron density in the substrate to overcome unfavorable ground-state equilibria.
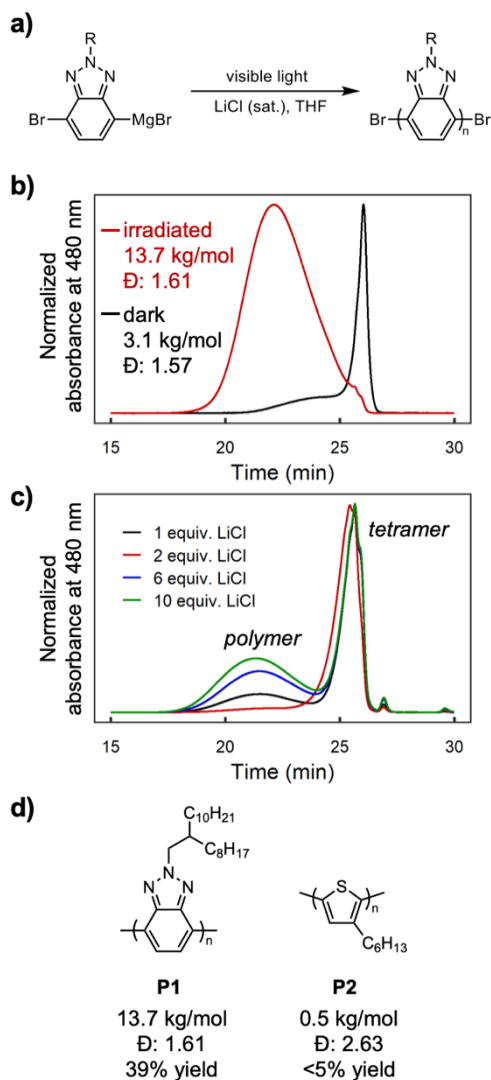
Figure 1. a) Gel permeation chromatography (GPC) traces of photopolymerization of **P1** using conditions from ref 13, with and without light. b) GPC traces showing the effect of LiCl on polymer molecular weight distribution for the photopolymerization of **P1**. Low molecular weight species is **P1** tetramer; see ref. 13 for details. c) Representative n-type (**P1**) and p-type (**P2**) polymers obtained via photopolymerization.

Results and Discussion

Propagating polymer chains are bromide-capped radical anions

First, we sought to experimentally determine the nature of the growing polymer chain in the reaction. Polymers isolated by precipitation into methanol from the photopolymerization of **P1** exhibit a mixture of Br/Br, Br/H, and H/H chain ends by MALDI-TOF-MS (Figure S2). However, dynamic equilibria of Grignard species in

solution complicate this analysis.[19-21] To better characterize the active chain-end of growing polymers during the reaction, we designed an in-situ aldehyde chain-trapping experiment (Scheme 2).

Scheme 1: Proposed mechanism of the coupling between aryl Grignard reagents and aryl halides
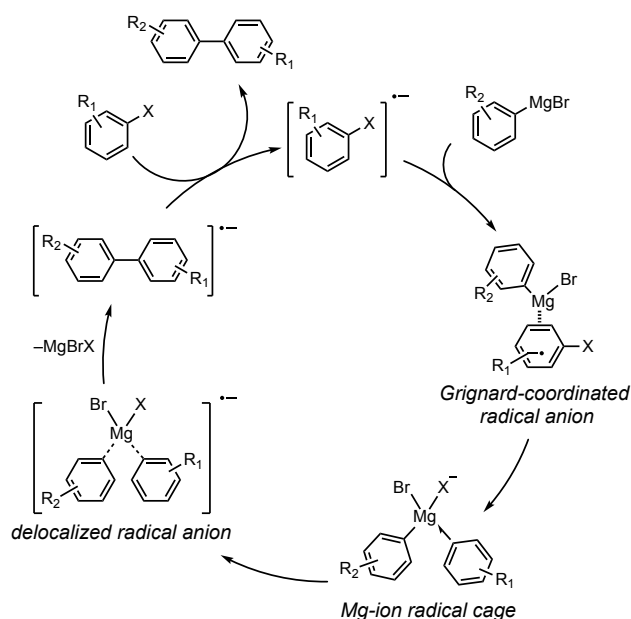
4,7-Dibromo-2-(2-octyldodecyl)-2H-benzo[d][1,2,3]triazole (**1**) was converted to a mono-Grignard reagent (**1-MgBr**) and subjected to standard photopolymerization conditions (see ref 13 for details). After four hours of irradiation, at which point polymers are still propagating, 2,6-difluorobenzaldehyde was injected into the polymerization. The reaction allowed to continue for 20 hours prior to quenching by precipitation into methanol. Fractionation of the reaction by precipitation into acetone shows no incorporation of the fluorinated aldehyde by ^{19}F NMR in either polymer or oligomer fractions (Figure S5). Concentration of supernatant yielded the small-molecule products, which showed a new ^{19}F NMR signal distinct from 2,6-difluorobenzaldehyde. This new product was isolated and determined to be the product of Grignard monomer addition to the aldehyde (**3**) (see SI for details). These results suggest that the propagating polymers are capped by bromine, not magnesium. The Br/Br chain-ends likely come about through an initial oxidative dimerization of Grignard monomers mediated by adventitious oxygen, as has been previously reported in the literature.[22–24] The literature conditions for oxidative dimerization could indeed be reproduced using the Grignard monomer (see SI for details). We hypothesize that protonated chain ends, observed by MALDI-TOF-MS, result from Grignard metathesis between monomer and polymer chains, a possible termination pathway for the polymerization.

Scheme 2: Aldehyde chain-end capping experiment.
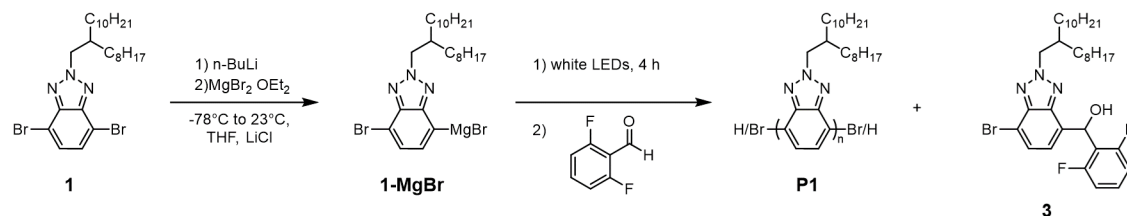
Having identified the chain ends, we then went on to characterize the electronic state of the growing polymer. The mechanistic study by Haines and Wiest proposed that the reaction is propagated by aryl halide radical anions.[18] Given the evidence of brominated chain-ends, if the growing polymers were found to be radical anions, it could suggest that the polymerization operates under a similar mechanism. Indeed, continuous-wave electron paramagnetic resonance (CW-EPR) of the polymerization shows radical character (Figure 2). CW-EPR of **1-MgBr** before irradiation shows no signal, suggesting that the radical character seen in the reaction is associated with the polymer. Isolated **P1** also shows no radical character by CW-EPR, but **P1** treated with of sodium naphthalenide (1 equivalent per polymer chain) show a similar EPR signal, further suggesting that radical character must be associated with the polymer chains (see SI, Figures S22-23 for fitting). Taken together, the chain-end capping and CW-EPR experiments suggest that the growing polymer chains are bromine-capped radical anions.
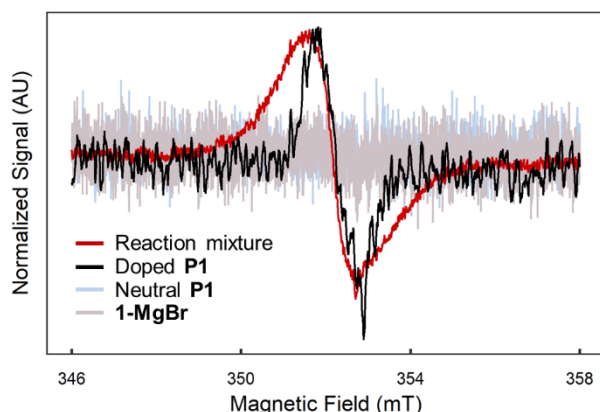

Figure 2. Continuous wave electron paramagnetic resonance spectra of neutral **P1**, chemically reduced **P1**, **1-MgBr**, and polymerization reaction mixture of **P1** (see SI for details).

LiCl prevents monomer coordination to heteroatoms along the polymer chain

With a better understanding of the identity of the growing polymer chain, we began our computational investigation using density functional theory (DFT, CAM-B3LYP/6-311G(d) CPCM (THF)) calculations,[25] initially using the dibrominated benzotriazole dimer radical anion as a model. Three major coordination modes of the monomer to the radical anion were located (Figure 3a). The two lowest-energy coordination modes are at the chain-end nitrogen (**4**) and internal nitrogen (**5**) positions of the benzotriazole ring. Coordination to the π-system of the aromatic ring (**6**), which is required for abstracting the chain-end bromine, is 9.3 and 7.0 kcal/mol higher in free energy than the nitrogen-coordinated structures **4** and **5**, respectively. These data suggest that nitrogen coordination could be a significant unproductive trap for the Grignard monomer.

We hypothesized that LiCl could coordinate the nitrogen atoms and free up the Grignard monomer for productive reactions. Indeed, we found that a THF-solvated lithium cation can displace the Grignard monomer from chain-end nitrogen sites in a model reaction ($\Delta G° = -11.1$ kcal/mol, Figure 3b). It should be noted that the difference in energy predicted by this model reaction is likely overestimated due to inaccuracies in the solvation energy of the free Li^+ by the hybrid explicit solvation/CPCM implicit solvation model. Previous performance studies of the CPCM implicit solvent model suggest the mean absolute deviation in solvation energies is 3-5 kcal/mol.[26] Even accounting for this error, the computed energy suggests that solvated Li^+ can displace the Grignard monomer from the chain-end nitrogen sites of the dimer radical anion. These calculations suggest that superstoichiometric quantities of LiCl improve the reaction by pushing this equilibrium further to the right, saturating the nitrogen "trap" sites on the polymer to disfavor unproductive monomer binding.

Recent computational studies of aryl Grignard reagents have revealed stable dimeric aggregates that sequester reactive monomer and push the equilibrium away from the chain-bound structures required in our proposed mechanism.[27] We identified two such dimeric aggregates for **1-MgBr** (Figure S20). These structures are >18 kcal/mol less stable than the bis-solvated monomer, likely due to the increased sterics of the benzotriazole structure compared to previously studied systems. Furthermore, the addition of stoichiometric LiCl to Grignard reagents is known to greatly enhance reactivity through the formation of "turbo Grignards" that are proposed to disrupt aggregation.[28,29] Therefore, in addition to blocking nitrogen sites on the growing chain, LiCl may also have a secondary role limiting unproductive aggregation of the monomer. Taken together, we do not believe that Grignard aggregates are a significant contributor to the proposed mechanism, and our model studies focus on interactions between monomeric Grignard reagents with the polymer chain.
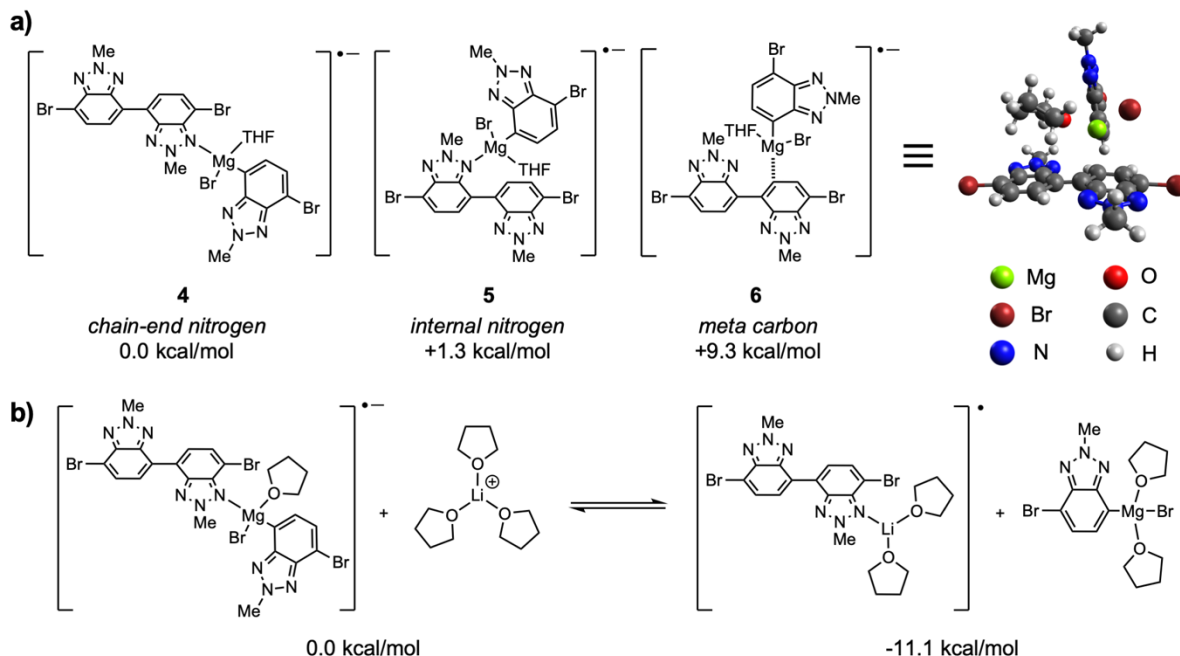
Figure 3. a) Structures of the Grignard monomer coordinated to the benzotriazole dimer radical anion (of the carbon coordination modes, the meta-carbon is the lowest energy). Gibbs free energies are relative to chain-end nitrogen coordination. b) Computed relative Gibbs free energy for the equilibrium between monomer versus lithium cation coordination at chain-end nitrogen sites on the benzotriazole radical anion dimer.

Energy landscape of dimer C–Br scission and C–C formation

As the forward reaction requires the Grignard at the chain end to abstract bromide, we investigated the energy landscape as the monomer approaches the C–Br bond in the radical anion dimer (Figure 4a). It should be noted that Mg coordination to the aromatic ring occurs via an η^1 binding mode, as discussed in energy landscape. A transition state, **TS-1**, was identified along the reaction pathway between monomer bound to the meta position in **6** and an ipso-coordinated structure (**8**). Intrinsic reaction coordinate analysis of **TS-1** connects to an *ortho*-coordinated structure (**7**). Frequency analysis shows that **7** is not a local minimum, instead falling to **6** upon optimization. This analysis suggests the process of monomer migration to the ipso carbon can proceed carbon-by-carbon along the ring. Geometric analysis of **TS-1** indicates that the migration is coupled with concomitant bending of the C–Br bond (164° out of aryl plane). A similar bending was observed in the small-molecule study and can be attributed to the intra-molecular electron transfer of the unpaired electron from the π system to the C–Br σ* orbital.[18,30–36] Overall, the migration of the Grignard to the ipso carbon requires a barrier of 9.4 kcal/mol. Alternatively, as the energies for 6 and 8 coordination are close in energy ($\Delta G° = 0.7$ kcal/mol), it is possible that monomer could directly coordinate to the ipso carbon from solution.

From **8**, there is a small barrier of 4.2 kcal/mol to break the carbon bromine bond (**TS-2**) and reach a Mg-ion-radical cage complex (**9**). A spin density map of **9** (Figure 4a, inset) shows that the radical is localized onto the ipso carbon of the dimer. As shown in Figure 4b, there is a 0.7 kcal/mol barrier for the aryl ring of the monomer of **9** to rotate (**TS-3**), allowing delocalization of the unpaired electron across the two aryl systems through Mg (**10**, spin density Figure 4b inset). The delocalized radical structure then passes through another low barrier of 3.1 kcal/mol (**TS-4**) to form the new C–C bond. The small barriers of all steps related to C–C bond formation suggest that once formed, **9** is rapidly converted to product, explaining why rapid termination due to free sp² radicals is not observed.

The favorable coordination between Li⁺ and nitrogen in the dimer radical anion would indicate that the steps in Figure 4 likely occur through a combination of pathways involving Li⁺ coordination at different sites along the chain. Unfortunately, the additional computational expense of evaluating all possible Li-coordinated structures in the C–Br cleavage and C–C formation energy landscape proved prohibitive.

Light promotes propagation by shifting electron density towards the chain end

The energetics of the steps shown in Figures 4 for the dimer suggest that the processes of breaking the chain-end C–Br bond and forming the new C–C bond are thermodynamically favorable, with low kinetic barriers. From this energy landscape, light does not appear to be necessary for these steps. Indeed, our control experiments suggest that the first several monomer additions (up to DP 4) can occur without light.[13] We therefore turned our attention to chains of longer length to understand the role of light in the polymerization. We hypothesized that internal positions of the growing polymer chain could compete with the chain end for monomer coordination. These interactions will become increasingly important as the polymer chain grows, and the number of potential unproductive binding sites for the monomer increases.
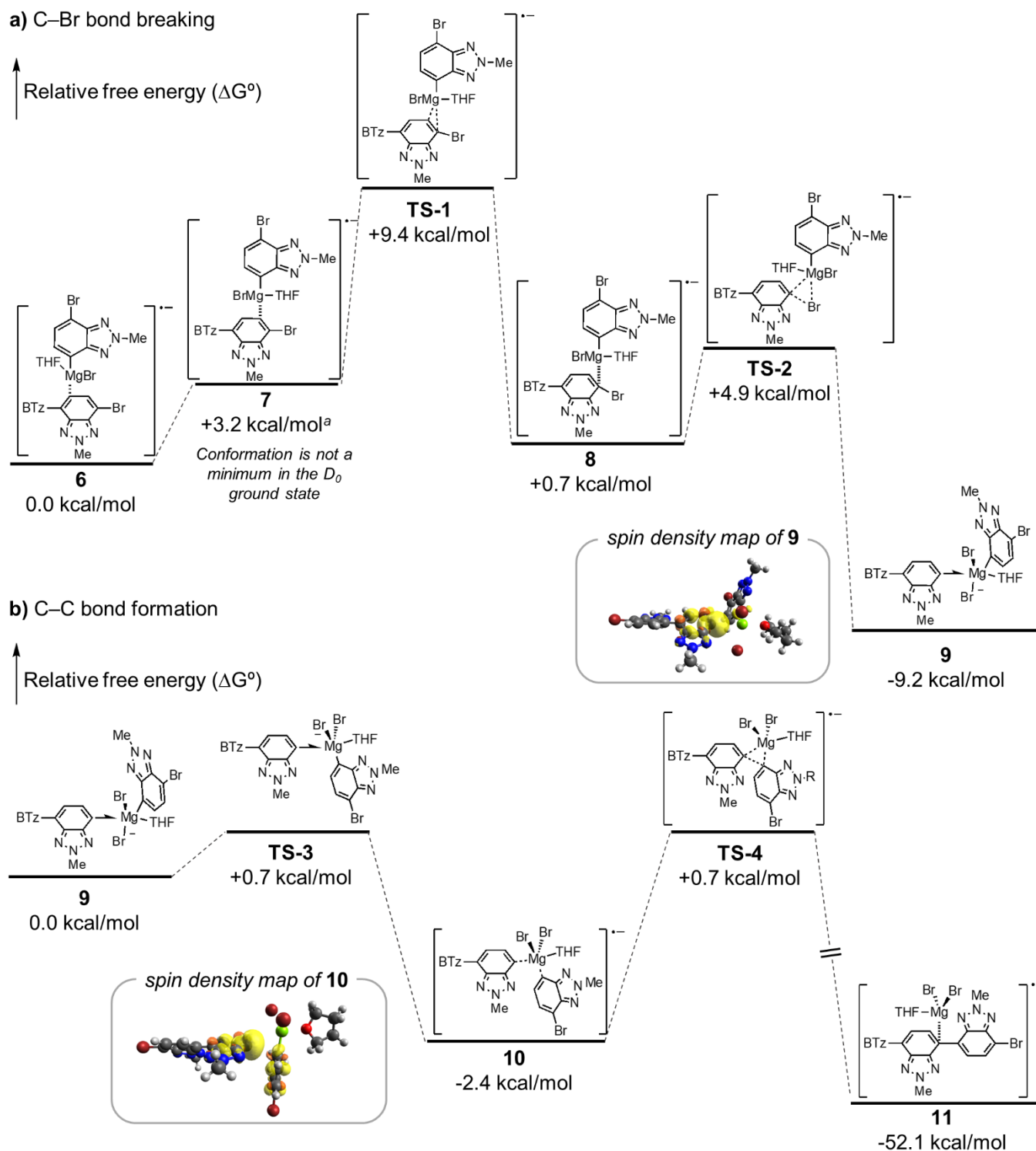
Figure 4. Benzotriazole dimer radical anion free energy surface for a) C–Br bond breaking and b) C–C bond formation. Drawn structures have the second monomer ring truncated with "BTz" (see SI for full structures). [a] The energy of this structure was estimated via constrained geometry optimization of the Mg–ipso carbon distance obtained from the IRC calculation of **TS-1**.
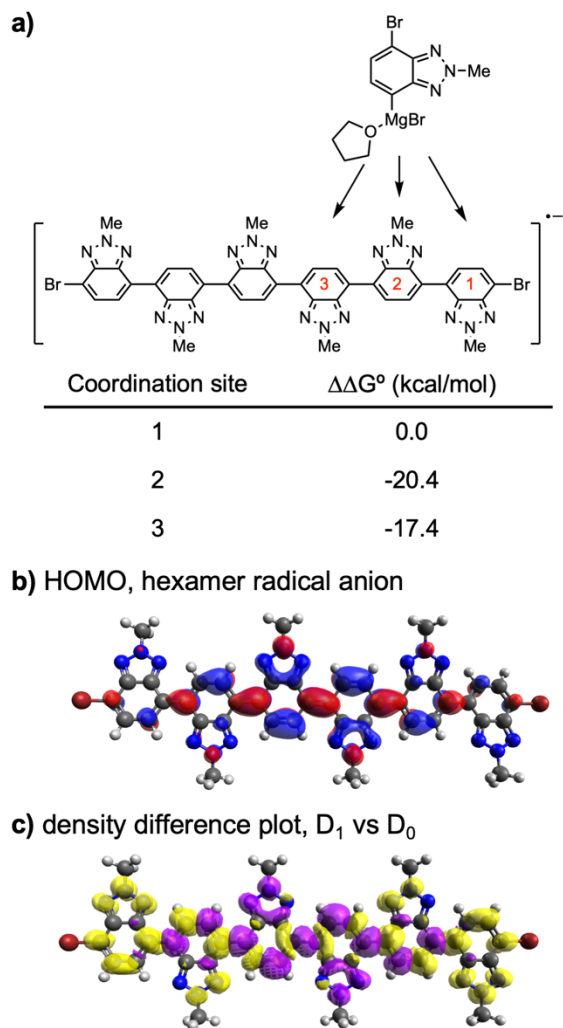
Figure 5. a) Relative Gibbs free energies of carbon-coordinated Grignard monomer complexes along the **P1** hexamer radical anion backbone, calculated relative to coordination at site 1 (for full structures, see Figure S13). b) HOMO of hexamer radical anion. c) Density difference plot of the first excited state (D_1) of the hexamer radical anion compared to the ground state. Yellow indicates a relative increase (D_1 vs D_0) of electron density, and violet indicates a relative decrease.

Based on studies of **P1** by Seferos,[37] we used the benzotriazole hexamer to model a polymer that has reached the effective conjugation length. We identified three carbon-centered η^1 monomer coordination structures for the hexamer radical anion (Figure S12). Attempts to coordinate the monomer to other positions along the hexamer resulted in either collapse to nitrogen coordination modes, or a return to these three structures. We find that in the hexamer, monomer binding to the chain end is no longer favorable in the ground state (Figure 5). Binding to internal monomer units is >17 kcal/mol more favorable than the chain-end benzotriazole (Figure 5a). This large difference in stability can be rationalized by visualizing the HOMO of the hexamer radical anion (Figure 5b), which shows significant localization of electron density on the inner monomer units.

This shift of electron density away from the chain ends has been previously observed in studies of n-doped CPs and is attributed to the stabilization provided when excess charge resides at the site of longest conjugation.[38–40]

To better understand the binding of monomers to the hexamer radical anion, we examined the enthalpies and entropies associated with each coordination site (Table S2; see SI for details). Coordination of the monomer to the chain end (site 1) requires significant polarization of the HOMO away from the center of the chain (Figure S13). Moving the negative charge away from the area of longest effective conjugation results in an enthalpic penalty. Additionally, binding at site 1 and charge reorganization is accompanied by the formation of a quinoidal structure at the chain end (Table S1). The increased double-bond character between the benzotriazole rings restricts rotation and results in a large entropic penalty for binding. In contrast, monomer binding at the inner rings (sites 2 and 3) is not accompanied by significant changes in bond lengths compared to the free hexamer radical anion.

These calculations suggest that as the chain grows, the Grignard monomer preferentially binds at internal sites. Because propagation can only occur when the monomer binds the chain end, the thermal polymerization stalls. To investigate how light promotes polymerization, we next examined the excited states of the hexamer radical anion. We performed time-dependent density functional theory (TD-DFT) calculations to visualize the electronic excitations of the hexamer radical anion to its lowest excited state (the D_1 doublet state). Density difference plots comparing the electron density in the ground and first excited state (D_0 and D_1 respectively) show a clear shift in electron density away from the internal monomer units and towards the chain ends (Figure 5c). Moreover, excited-state optimizations of the Grignard monomer bound to the hexamer radical anion converge to a structure with the monomer bound to the ortho-position of site 1, suggesting that the shift in electron density translates to changes in monomer coordination (Figure S14).

Thus, the role of light in the photopolymerization can be understood: light does not directly promote bond-breaking or bond formation, but instead favors productive monomer coordination (Scheme 3). To evaluate whether monomer must be pre-coordinated to the chain prior to photoexcitation, or whether a free excited-state chain could react with unbound monomer, we measured the excited-state lifetime of the **P1** radical anion. Femtosecond transient absorption spectroscopy of **P1**$^{\cdot-}$ reveals an excited-state lifetime of 850 ± 6 ps (Figure S15). The decay of this excited state would be competitive with molecular diffusion to form an encounter complex.[41,42] Therefore, we propose that the monomer pre-complexes to the chain before photoexcitation. After monomer coordination to the inner units of the ground-state polymer chain, photoexcitation shifts electron density to the chain end. This shift in electron density triggers monomer migration to the polymer chain end. Based on the low barriers predicted in the dimer model system (4.2 kcal/mol), C–Br cleavage should occur readily once the monomer reaches the chain end from either the D_1 state (Scheme 3a) or after relaxation to the kinetically trapped chain-end ground state, a local minimum (Scheme 3b).

Scheme 3: Proposed role of light in promoting propagation by directing monomer coordination to the chain end.
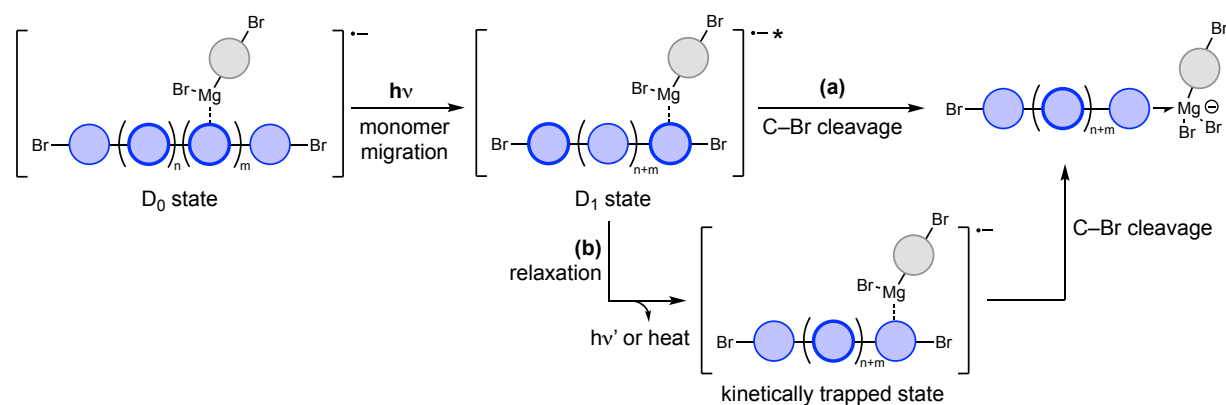

This proposal is consistent with experimental observations of light dependence. In dark controls, low-molecular-weight oligomers are formed at room temperature, in agreement with the low barriers observed in the dimer energy landscape. Formation of higher-molecular-weight polymers requires light (Figure 1b).[13] Visualization of HOMOs of the dimer, tetramer, and hexamer show a trend of increasing localization of electron density within the center for the chain as the length of conjugation increases (Figure S11). Excited-state geometry optimizations of the D_1 state for benzotriazole dimer and tetramer radical anions bound to monomer also show ortho-coordinated structures, suggesting that light could have a beneficial effect on the reaction even before polymers reach their effective conjugation length.

Estimation of the quantum yield (QY, defined here as the ratio of monomers consumed to photons absorbed by the reaction solution) over the course of the reaction suggests that the QY decreases from an initial value of 3.9% to a plateau of 1.6% after ~20% conversion (Figure S19). This decrease in QY can be ascribed to the formation of highly absorbing CP products, which creates an internal filter effect. Based on the proposed role of light in the mechanism, we also envision that as the chain grows, multiple irradiation steps may be required to fully "walk" the monomer to the chain end.

Summary of proposed propagation mechanism

Based on our computational and experimental results, we propose the following mechanism for propagation (Scheme 4). In the first step, the Grignard monomer samples coordination sites along the ground-state radical anion polymer chain, with Li^+ ions (not shown) blocking the N sites (Scheme 4, I). Photoexcitation of the polymer chain shifts electron density away from the inner monomer units towards the chain termini, directing monomer coordination to the reaction sites (Scheme 4, II). Once at the chain end, there are only small kinetic barriers for the Grignard monomer to direct the abstraction of the chain-end bromine (Scheme 4, III). The resulting Mg-radical ion cage complex then quickly collapses into a delocalized biaryl radical ion (Scheme 4, IV) that then forms the C–C bond while expelling $MgBr_2$ (Scheme 4, V).

Scheme 4: Proposed mechanism for propagation in the photo-polymerization of 1-MgBr.
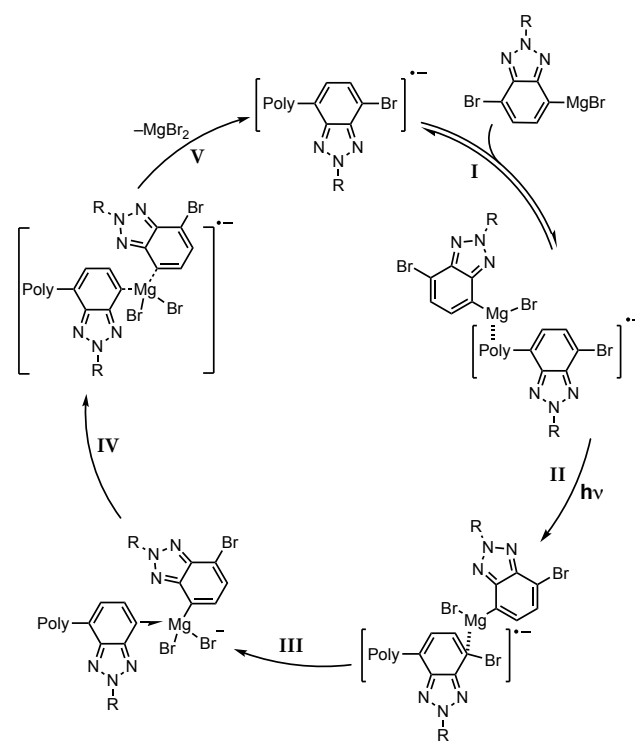
Recent computational studies of Grignard solvates and their reactivities suggest that there are likely many structures of the Grignard monomer in solution, which are nearly degenerate in energy.[27,43] A study by Cascella relating these structures to reactivity with carbonyl electrophiles found <2 kcal/mol difference between monomeric and dimeric solvates, suggesting that Grignard reactions may occur via an amalgamation of similar mechanisms.[43] Regardless of the many nuances of Grignard speciation in the experimental system, we believe that the mechanism in Scheme 4 provides a general framework for understanding the photopolymerization.

Benzotriazole is considered a weak acceptor,[44-46] but the photopolymerization tolerates more electron-poor and slightly more electron-rich monomers.[13] Key features of the **1-MgBr** system are present in the other successful monomer systems reported by us previously. The homopolymer poly(2,3-bis(2-ethylhexyl)thieno[3,4-b]pyrazine) has an electron-poor π-system and heteroaromatic sites

that could compete for Grignard coordination. Benzothiadiazole and diketopyrrolopyrrole based donor-acceptor monomers that were compatible with the polymerization, albeit producing low-molecular-weight polymers, also contain these key features. Thus, we anticipate this mechanistic framework will be relevant to the photopolymerization of other electron-deficient heteroaromatic CPs.

This light-promoted, Mg-templated $S_{RN}1$ reaction may be contrasted to the state-of-the-art in controlled CP synthesis, catalyst-transfer polycondensation (CTP).[10,47] Like CTP, the photopolymerization mechanism requires coordination of an organometallic species to the π-system of the growing polymer chain, although the interaction of the Grignard monomer with the radical anion chain is electrostatic in nature rather than π-backbonding.[48-50] Unlike CTP, however, the coordination does not need to be maintained throughout propagation to enforce a chain-growth mechanism; selective photoexcitation and residence of the radical anion along the growing chain favor chain growth over monomer-monomer coupling. However, uncontrolled initiation by adventitious oxygen and termination by Grignard metathesis remain drawbacks of our photopolymerization.

This work illustrates a highly unusual role for visible light in modulating the substrate electronics to promote productive binding, and an alternative to more common triplet sensitization and single-electron-transfer mechanisms. As CTP also relies on coordination of organometallic species to the polymer chain, we anticipate that this insight will inspire the development of photo-mediated variants.

Free-radical reactivity terminates electron-rich polymers

With this mechanistic framework for the successful **P1** system, we can now begin to investigate the poor reactivity of electron-rich monomers in the photopolymerization. Polythiophene is a ubiquitous p-type polymer in the literature, often synthesized by Pd- or Ni-catalyzed polycondensation, but under our standard reaction conditions, **2-MgBr** produces <5% yield of oligomers (Figure 6a). To understand why this reaction fails, we performed calculations for monomer coordination to the thiophene dimer radical anion, **12** (Figure 6a; the hexyl chain is truncated to CH_3), which would be produced by oxidative dimerization of the corresponding Grignard monomer. Recent computational work by Zimmerman on the aggregation of thiophene Grignard reagents suggests that thiophenes such as **2-MgBr** form stable solvate dimers.[27] Such dimers would decrease reactivity by pushing the equilibrium away from the necessary monomer-coordinated radical anions. For the purposes of our model study, we will focus on the interactions of monomeric thiophene Grignard reagents with the dimer radical anion **12**, but we acknowledge that monomer aggregation could also contribute to the low reactivity of electron-rich monomers in the photopolymerization.

The radical anion **12** shows C3 coordination analogous to **6** (Figure S10), in addition to a sulfur-coordinated structure **13** (Figure 6b). The sulfur-coordinated structure **13** is 2.4 kcal/mol more stable than the lowest-energy carbon-coordinated structure, suggesting that **13** represents the predominant form in solution. While the carbon-coordinated structures do not exhibit significant lengthening or bending of the C–Br bond, the sulfur-coordinated conformer exhibits C–Br bond elongation by 0.75 Å and significant spin density localization onto the carbon atom (Figure 6d; see Figure S10 for spin density maps of carbon-coordinated structures). The extent of bond breaking in this structure suggests that the electron-rich bithiophene

radical anion could be undergoing bond heterolysis, analogous to a typical $S_{RN}1$ reaction. If this is the case, the resulting "free" heteroaryl radical would likely undergo rapid hydrogen-atom abstraction from the weak C–H bonds of the THF solvent.

To test this hypothesis and the physical significance of the sulfur-coordinated structure, the photopolymerization of **2-MgBr** was conducted in parallel in either THF-d_8 or THF (Figure 7). Quenched and isolated oligomers from each reaction (n=3) show a clear +1 m/z shift by MALDI-TOF-MS that is consistent with deuterium incorporation. D incorporation is additionally observed by ^{2}H NMR for the THF-d_8 reaction, but not in THF (Figure 7). In contrast, when **1-MgBr** is polymerized in THF-d_8, no deuterium incorporation is seen by ^{2}H NMR (Figure S8) or MALDI-TOF-MS (Figure S7).
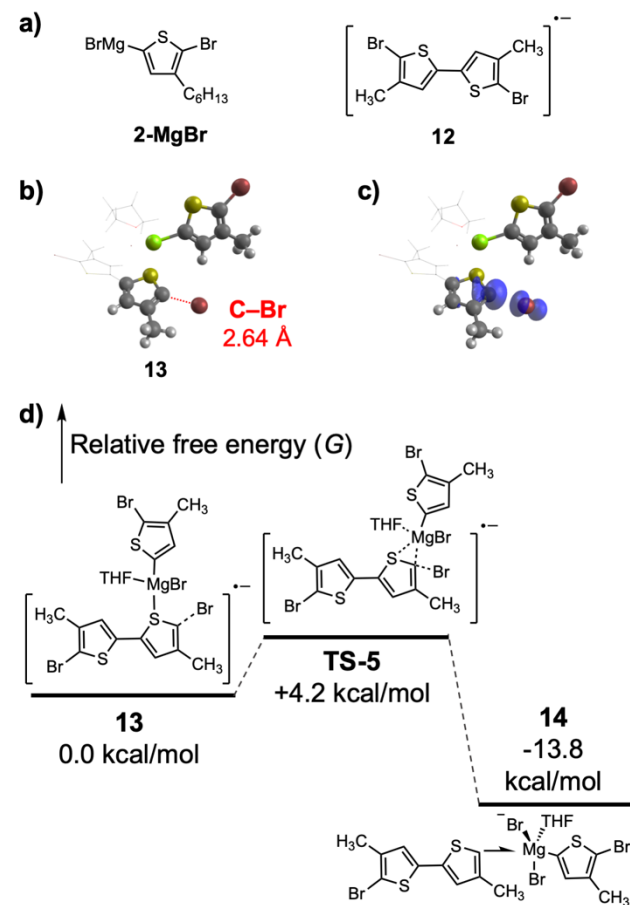

Figure 6. a) Structures of monomer **2-MgBr** and the bithiophene radical anion **12**, used as a model system for calculations. b) Calculated structure of **13**; coordination at S is the lowest-energy coordination structure and results in 0.75 Å elongation of the C–Br bond. The explicitly coordinated THF, Br and second thiophene ring have been represented in wireframe for clarity. c) Spin density map (isovalue 0.005) for the sulfur-coordinated conformer **13**. d) Relative Gibbs free energy landscape of C–Br abstraction in the thiophene dimer model system, and structures of **TS-5** and **14**.

Furthermore, computational analysis of C–Br cleavage from **13** shows that electron-rich systems could be compatible with the photopolymerization conditions, if the termination process can be prevented. A transition state structure (Figure 6d, **TS-5**) was identified for the thiophene dimer connecting **13** to a Mg-ion radical cage, **14** (analogous to **9**). There is a 4.2 kcal/mol free energy barrier from **13**

to **TS-5,** consistent with the barrier from benzotriazole dimer **8** to **TS-2**.

Our previous work showed that other polymers with sulfur heteroatoms, including poly(thienopyrazine) and donor-acceptor alternating copolymers containing thiophenes as the donor, were compatible with the photopolymerization, suggesting that this termination cannot be attributed to sulfur coordination alone.[13] Like thiophene, an electronically neutral hydrocarbon monomer 2,7-dibromo-9,9-dioctyl-9H-fluorene produced only trace oligomer.[13] Computational modeling of monomer coordination to a fluorene dimer radical anion also showed bromine abstraction and dissociation of the Grignard reagent, suggesting that C–Br bond scission to form free radicals is primarily related to monomer electronics (Figure S21). Taken together, the computed dimer radical anion structures and THF-d_8 reactions suggest that electron-neutral and -rich monomers fail under the photopolymerization conditions due to $S_{RN}1$ pathways that form rapidly terminated free sp^2 radicals.
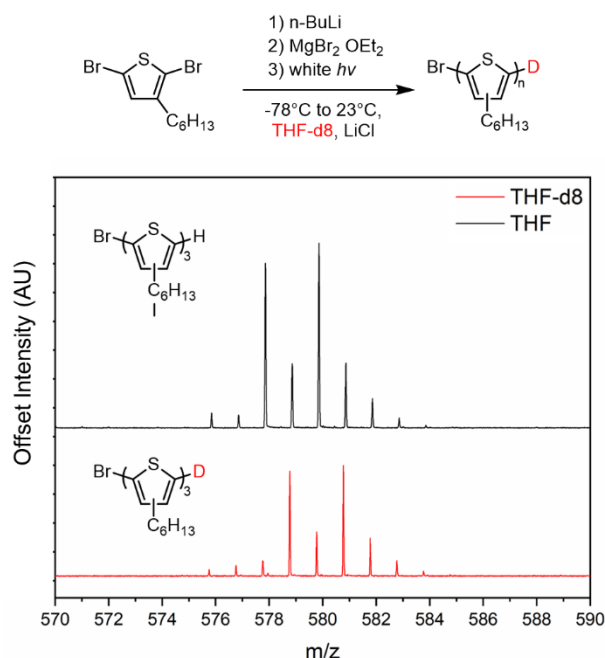

Figure 7. Photopolymerization of 2,5-dibromo-3-hexylthiophene in THF-d_8 (top) and MALDI-TOF-MS comparison of isolated trimer from THF-d_8 polymerization and THF polymerization.

Conclusion

In summary, we have experimentally and computationally explored the photopolymerization of aryl Grignard monomers. These studies reveal a Mg-templated $S_{RN}1$ reaction analogous to the thermal small-molecule version, but explain why thermal conditions fail to produce CPs. Our calculations suggest that for electron-deficient heteroaromatic monomers, once the Grignard monomer coordinates to the polymer chain end, the barriers to bromide abstraction and C–C bond formation are exceptionally low. The rapid rate of these steps and delocalization of the radical intermediate minimizes side reactions that would be expected for free sp^2 radicals in a traditional $S_{RN}1$ process. The extended π-system of the growing polymer chain and abundance of coordinating heteroatoms necessitate key modifications to the thermal small-molecule reaction: irradiation by visible light and excess LiCl. In combination, LiCl and light funnel Grignard monomers to the reactive chain-end sites. High

concentrations of LiCl block the heteroatom sites of the polymer chain, promoting Grignard monomer coordination along the pi-system of the polymer backbone. As the chain grows, unproductive Grignard monomer binding to inner sites of the polymer backbone dominate, and photoexcitation is required to shift electron density to the chain ends and favor productive binding events. Furthermore, this mechanistic study provides insight into the incompatibility of electron-rich and -neutral monomers with the photopolymerization. These radical anions undergo facile C–Br heterolysis, resulting in unstabilized sp^2 radicals that undergo termination by H-atom abstraction. Future work will focus on using these mechanistic insights to increase the yields and molecular weights obtainable by photopolymerization. *In silico* insights into the failure of electron-rich and -neutral monomers will enable the design of monomers and organometallic reagents that are compatible with this reaction and produce high-performance CPs. Furthermore, understanding the mechanisms of initiation and termination will allow us to devise conditions with better control over the polymerization.

ASSOCIATED CONTENT

Supporting Information.

Synthetic procedures; details of the computational methods; characterization data for new compounds; visualized HOMO and LUMOs of relevant structures; XYZ coordinates of calculated structures. This material is available free of charge via the Internet at http://pubs.acs.org.

AUTHOR INFORMATION

Corresponding Authors

* Julia A. Kalow – Department of Chemistry, Northwestern University, Evanston Illinois 60208
* Brandon E. Haines – Department of Chemistry, Westmont College, Santa Barbara, CA 93108.

REFERENCES

(1)   Xu, S.; Kim, E. H.; Wei, A.; Negishi, E. I. Pd- and Ni-Catalyzed Cross-Coupling Reactions in the Synthesis of Organic Electronic Materials. *Science and Technology of Advanced Materials*. Taylor & Francis 2014.

(2)   Usluer, Ö.; Abbas, M.; Wantz, G.; Vignau, L.; Hirsch, L.; Grana, E.; Brochon, C.; Cloutet, E.; Hadziioannou, G. Metal Residues in Semiconducting Polymers: Impact on the Performance of Organic Electronic Devices. *ACS Macro Lett.* **2014**, 3, 1134–1138.

(3)   Bannock, J. H.; Treat, N. D.; Chabinyc, M.; Stingelin, N.; Heeney, M.; de Mello, J. C. The Influence of Polymer Purification on the Efficiency of Poly(3-Hexylthiophene):Fullerene Organic Solar Cells. *Sci. Rep.* **2016**, *6*, 23651.

(4)   Krebs, F. C.; Nyberg, R. B.; Jørgensen, M. Influence of Residual Catalyst on the Properties of Conjugated Polyphenylenevinylene Materials: Palladium Nanoparticles and Poor Electrical Performance. *Chem. Mater.* **2004**, *16*, 1313–1318.

(5)   Kuwabara, J.; Yasuda, T.; Takase, N.; Kanbara, T. Effects of the Terminal Structure, Purity, and Molecular Weight of an Amorphous Conjugated Polymer on Its Photovoltaic Characteristics. *ACS Appl. Mater. Interfaces* **2016**, *8*, 1752–1758.

(6)   Liu, X.; Sharapov, V.; Zhang, Z.; Wiser, F.; Awais, M. A.; Yu, L. Photoinduced Cationic Polycondensation in Solid State towards Ultralow Band Gap Conjugated Polymers. *J. Mater. Chem. C* **2020**, *8*, 7026–7033.

(7)   Koyuncu, S.; Hu, P.; Li, Z.; Liu, R.; Bilgili, H.; Yagci, Y. Fluorene-Carbazole-Based Porous Polymers by Photoinduced Electron Transfer Reactions. *Macromolecules* **2020**, *53*, 1645–1651.

(8)   Celiker, T.; İsci, R.; Kaya, K.; Ozturk, T.; Yagci, Y. Photoinduced Step-growth Polymerization of Thieno[3,4-b] Thiophene Derivatives. The Substitution Effect on the Reactivity and Electrochemical Properties. *J. Polym. Sci.* **2020**, *58*, 2327–2334.

(9)   Woods, E. F.; Berl, A. J.; Kalow, J. A. Advances in the Synthesis of π-Conjugated Polymers by Photopolymerization. *ChemPhotoChem* **2021**, *5*, 4–11.

(10)   Leone, A. K.; McNeil, A. J. Matchmaking in Catalyst-Transfer Polycondensation: Optimizing Catalysts Based on Mechanistic Insight. *Acc. Chem. Res.* **2016**, *49*, 2822–2831.

(11)   Leone, A. K.; Mueller, E. A.; McNeil, A. J. The History of Palladium-Catalyzed Cross-Couplings Should Inspire the Future of Catalyst-Transfer Polymerization. J. Am. Chem. Soc. 2018, 140, 15126–15139.

(12)   Jia, H.; Lei, T. Emerging Research Directions for N-Type Conjugated Polymers. *J. Mater. Chem. C* **2019**, *7*, 12809–12821.

(13)   Woods, E. F.; Berl, A. J.; Kalow, J. A. Photocontrolled Synthesis of N-Type Conjugated Polymers. *Angew. Chemie Int. Ed.* **2020**, *59*, 6062.

(14)   Li-Yuan Bao, R.; Zhao, R.; Shi, L. Progress and Developments in the Turbo Grignard Reagent I-PrMgCl·LiCl: A Ten-Year Journey. *Chem. Commun.* **2015**, *51*, 6884–6900.

(15)   Ziegler, D. S.; Wei, B.; Knochel, P. Improving the Halogen–Magnesium Exchange by Using New Turbo-Grignard Reagents. *Chem. – A Eur. J.* **2019**, *25*, 2695–2703.

(16)   Uchiyama, N.; Shirakawa, E.; Hayashi, T. Single Electron Transfer-Induced Grignard Cross-Coupling Involving Ion Radicals as Exclusive Intermediates. *Chem. Commun.* **2013**, *49*, 364–366.

(17)   Murarka, S.; Studer, A. Radical/Anionic SRN1-Type Polymerization for Preparation of Oligoarenes. *Angew. Chemie Int. Ed.* **2012**, *51*, 12362–12366.

(18)   Haines, B. E.; Wiest, O. SET-Induced Biaryl Cross-Coupling: An SRN1 Reaction. *J. Org. Chem.* **2014**, *79*, 2771–2774.

(19)   Ashby, E. C.; Nackashi, J.; Parris, G. E. Composition of Grignard Compounds. X. NMR, Ir, and Molecular Association Studies of Some Methylmagnesium Alkoxides in Diethyl Ether, Tetrahydrofuran, and Benzene. *J. Am. Chem. Soc.* **1975**, *97*, 3162–3171.

(20)   Seyferth, D. The Grignard Reagents. *Organometallics* **2009**, *28*, 1598–1605.

(21)   Peltzer, R. M.; Eisenstein, O.; Nova, A.; Cascella, M. How Solvent Dynamics Controls the Schlenk Equilibrium of Grignard Reagents: A Computational Study of CH3MgCl in Tetrahydrofuran. *J. Phys. Chem. B* **2017**, *121*, 4226–4237.

(22)   Krasovskiy, A.; Tishkov, A.; del Amo, V.; Mayr, H.; Knochel, P. Transition-Metal-Free Homocoupling of Organomagnesium Compounds. *Angew. Chemie Int. Ed.* **2006**, *45*, 5010–5014.

(23)   Maji, M. S.; Pfeifer, T.; Studer, A. Oxidative Homocoupling of Aryl, Alkenyl, and Alkynyl Grignard Reagents with TEMPO and Dioxygen. *Angew. Chemie Int. Ed.* **2008**, *47*, 9547–9550.

(24)   Murarka, S.; Möbus, J.; Erker, G.; Mück-Lichtenfeld, C.; Studer, A. TEMPO-Mediated Homocoupling of Aryl Grignard Reagents: Mechanistic Studies. *Org. Biomol. Chem.* **2015**, *13*, 2762–2767.

(25)   Full geometry optimizations of stationary points were calculated at the CAM-B3LYP/6-311G(d)/CPCM(THF) level of theory. Energies reported for stationary points are Gibbs free energies calculated at 298 K and 1.0 M standard state. See SI for full details

(26)   Takano, Y.; Houk, K. N. Benchmarking the Conductor-like Polarizable Continuum Model (CPCM) for Aqueous Solvation Free Energies of Neutral and Ionic Organic Molecules. *J. Chem. Theory Comput.* **2005**, *1*, 70–77.

(27)   Curtis, E. R.; Hannigan, M. D.; Vitek, A. K.; Zimmerman, P. M. Quantum Chemical Investigation of Dimerization in the Schlenk Equilibrium of Thiophene Grignard Reagents. *J. Phys. Chem. A* **2020**, *124*, 1480–1488.

(28)   Li-Yuan Bao, R.; Zhao, R.; Shi, L. Progress and Developments in the Turbo Grignard Reagent I-PrMgCl·LiCl: A Ten-Year Journey. *Chem. Commun.* **2015**, *51*, 6884–6900.

(29)   Ziegler, D. S.; Wei, B.; Knochel, P. Improving the Halogen–Magnesium Exchange by Using New Turbo-Grignard Reagents. *Chem. – A Eur. J.* **2019**, *25*, 2695–2703.

(30)   Pierini, A. B.; Duca, J. S. Theoretical Study on Haloaromatic Radical Anions and Their Intramolecular Electron Transfer Reactions. *J. Chem. Soc. Perkin Trans. 2* **1995**, *No. 9*, 1821–1828.

(31)   B. Pierini, A.; S. Duca, J.; Jr., Domingo M. A. Vera, J. S. D.; M. A. Vera, D. A Theoretical Approach to Understanding the Fragmentation Reaction of Halonitrobenzene Radical Anions†. *J. Chem. Soc. Perkin Trans. 2* **1999**, *No. 5*, 1003–1010.

(32)   Laage, D.; Burghardt, I.; Sommerfeld, T.; Hynes, J. T. On the Dissociation of Aromatic Radical Anions in Solution. 1. Formulation and Application to p-Cyanochlorobenzene Radical Anion. *J. Phys. Chem. A* **2003**, *107*, 11271–11291.

(33)   Burghardt, I.; Laage, D.; Hynes, J. T. On the Dissociation of Aromatic Radical Anions in Solution. 2. Reaction Path and Rate Constant Analysis. *J. Phys. Chem. A* **2003**, *107*, 11292–11306.

(34)   Pierini, A. B.; Vera, D. M. A. Ab Initio Evaluation of Intramolecular Electron Transfer Reactions in Halobenzenes and Stabilized Derivatives. *J. Org. Chem.* **2003**, *68*, 9191–9199.

(35)   Takeda, N.; Poliakov, P. V; Cook, A. R.; Miller, J. R. Faster Dissociation: Measured Rates and Computed Effects on Barriers in Aryl Halide Radical Anions. *J. Am. Chem. Soc.* **2004**, *126*, 4301–4309.

(36)   Costentin, C.; Robert, M.; Savéant, J.-M. Fragmentation of Aryl Halide π Anion Radicals. Bending of the Cleaving Bond and Activation vs Driving Force Relationships. *J. Am. Chem. Soc.* **2004**, *126*, 16051–16057.

(37)   McCormick, T. M.; Bridges, C. R.; Carrera, E. I.; DiCarmine, P. M.; Gibson, G. L.; Hollinger, J.; Kozycz, L. M.; Seferos, D. S. Conjugated Polymers: Evaluating DFT Methods for More Accurate Orbital Energy Modeling. *Macromolecules* **2013**, *46*, 3879–3886.

(38)   Wang, S.; Sun, H.; Ail, U.; Vagin, M.; Persson, P. O. Å.; Andreasen, J. W.; Thiel, W.; Berggren, M.; Crispin, X.; Fazzi, D.; Fabiano, S. Thermoelectric Properties of Solution-Processed n-Doped Ladder-Type Conducting Polymers. *Adv. Mater.* **2016**, *28*, 10764–10771.

(39)   Fazzi, D.; Fabiano, S.; Ruoko, T.-P.; Meerholz, K.; Negri, F. Polarons in π-Conjugated Ladder-Type Polymers: A Broken Symmetry Density Functional Description. *J. Mater. Chem. C* **2019**, *7*, 12876–12885.

(40)   Debnath, S.; Boyle, C. J.; Zhou, D.; Wong, B. M.; Kittilstved, K. R.; Venkataraman, D. Persistent Radical Anion Polymers Based on Naphthalenediimide and a Vinylene Spacer. *RSC Adv.* **2018**, *8*, 14760–14764.

(41)   Haimerl, J.; Ghosh, I.; König, B.; Vogelsang, J.; Lupton, J. M. Single-Molecule Photoredox Catalysis. *Chem. Sci.* **2019**, *10*, 681–687.,

(42)   Brandl, F.; Bergwinkl, S.; Allacher, C.; Dick, B. Consecutive Photoinduced Electron Transfer (ConPET): The Mechanism of the Photocatalyst Rhodamine 6G. *Chem. – A Eur. J.* **2020**, *26*, 7946–7954.

(43)   Peltzer, R. M.; Gauss, J.; Eisenstein, O.; Cascella, M. The Grignard Reaction – Unraveling a Chemical Puzzle. *J. Am. Chem. Soc.* **2020**, *142*, 2984–2994.

(44)   Patel, D. G. (Dan); Feng, F.; Ohnishi, Y.; Abboud, K. A.; Hirata, S.; Schanze, K. S.; Reynolds, J. R. It Takes More Than an Imine: The Role of the Central Atom on the Electron-Accepting Ability of Benzotriazole and Benzothiadiazole Oligomers. *J. Am. Chem. Soc.* **2012**, *134*, 2599–2612.

(45) Balan, A.; Baran, D.; Toppare, L. Benzotriazole Containing Conjugated Polymers for Multipurpose Organic Electronic Applications. *Polym. Chem.* **2011**, *2*, 1029–1043.

(46) Tanimoto, A.; Yamamoto, T. Synthesis of N-Type Poly(Benzotriazole)s Having p-Conducting and Polymerizable Carbazole Pendants. *Macromolecules* **2006**, *39*, 3546–3552.

(47) Bryan, Z. J.; Mcneil, A. J. Conjugated Polymer Synthesis via Catalyst-Transfer Polycondensation (CTP): Mechanism, Scope, and Applications. *Macromolecules* **2013**, *46*, 8395–8405.

(48) He, W.; Patrick, B. O.; Kennepohl, P. Identifying the Missing Link in Catalyst Transfer Polymerization. *Nat. Commun.* **2018**, *9*, 3866.

(49) Tkachov, R.; Senkovskyy, V.; Komber, H.; Sommer, J.-U.; Kiriy, A. Random Catalyst Walking along Polymerized Poly(3-Hexylthiophene) Chains in Kumada Catalyst-Transfer Polycondensation. *J. Am. Chem. Soc.* **2010**, *132*, 7803–7810.

(50) Leone, A. K.; Goldberg, P. K.; McNeil, A. J. Ring-Walking in Catalyst-Transfer Polymerization. *J. Am. Chem. Soc.* **2018**, *140*, 7846–7850.

EPR

Normalized Signal (AU)

reaction
polymer + Na(Naph)

346   350   354   358
Magnetic Field (mT)

density difference plot, D_1 vs. D_0

experiment   **TD-DFT**